Photoemission of protons from beryllium and carbon in the energy range from 180 to 580 MeV

S. Homma, M. Kanazawa, K. Maruyama, Y. Murata, and H. Okuno
Institute for Nuclear Study, University of Tokyo, Tanashi, Tokyo 188, Japan

A. Sasaki
Faculty of Education, Akita University, Akita 010, Japan

T. Taniguchi*
Department of Physics, Hiroshima University, Hiroshima 730, Japan
(Received 25 May 1982)

Momentum spectra of protons in the reactions of $\gamma+\text{Be}\rightarrow p+$anything and $\gamma+\text{C}\rightarrow p+$anything were measured in the photon energy range from 180 to 420 MeV for beryllium and from 340 to 580 MeV for carbon by use of a tagged photon beam. The spectrum obtained shows two peaks which are interpreted to be due to the protons in the reactions $\gamma+\text{"}N\text{"}\rightarrow p+\pi$ and $\gamma+\text{"}pn\text{"}\rightarrow p+n$, where "$N$" and "$pn$" are the quasifree nucleons and proton-neutron systems in the target nuclei.

I. INTRODUCTION

A high energy photon seems to be a good probe for investigating the microscopic structure of the nucleus. The reasons are that the nucleus can be studied with a spatial resolution determined by the wavelength of the photon, and since the photon interacts through the electromagnetic interaction, serious distortions of the nucleus are not induced by the probe.

At energies above 200 MeV, the wavelength of the photon is less than the internucleon distance. This means that in analyzing the results of the photoproduction data at such energies we could reasonably assume that the photon interacts with one-nucleon or two-nucleon systems, if they exist, rather than with the entire nucleus as a whole.

Recently, a tagged photon in the energy region above 200 MeV was developed at the Tokyo[1] and Bonn[2] synchrotrons. The energy bin width of these photon beams is of the order of 10 MeV, which allows us to investigate nuclear structure with an energy resolution much smaller than the Fermi momentum of the individual nucleons in the nucleus.

In this paper, we present experimental cross sections for inclusive photoemission of protons from beryllium and carbon nuclei in the photon energy range between 180 and 420 MeV for beryllium, and between 340 and 580 MeV for carbon. Our main interest in this photoemission of protons from the nucleus is whether a quasifree nucleon peak in the momentum spectrum of protons exists or not, and also whether a quasifree "two-nucleon-system" peak in the momentum spectrum of protons exists or not. The existence of the latter peak may suggest a strong correlation between nucleons in the nucleus.

Up to now, data on the photoemission of protons from various nuclei have been accumulated by various authors, especially in the energy region below meson threshold. Since in this energy region photons are considered to be absorbed by the nucleus mainly through electric dipoles, the results of the photoemission of protons were usually analyzed by use of a phenomenological quasideuteron model developed by Levinger[3] and extended by Gottfried.[4] In its simplest form, this model describes a photonuclear reaction by the interaction between the incident photon and a correlated proton-neutron pair (quasideuteron) in the nucleus. In an extreme view of such a mechanism of photon absorption, we might imagine the fundamental absorbing system to consist of a proton-neutron cluster close together and unaffected by other nucleons in the nucleus. Since such a situation might be realized in the energy region above 200 MeV, we could expect a peak in the momentum spectrum of photoemitted protons due to the photodisintegration of such p-n pairs in the nucleus.

The experiment was performed using a photon tagging system at the 1.3 GeV electron synchrotron

31

at the Institute for Nuclear Study, University of Tokyo. The preliminary results have been published elsewhere.[5]

II. EXPERIMENT

The experiment to measure the momentum spectrum of protons in the reactions,

$$\gamma + {}^9\mathrm{Be} \rightarrow p + \text{anything} \tag{1}$$

and

$$\gamma + {}^{12}\mathrm{C} \rightarrow p + \text{anything} \tag{2}$$
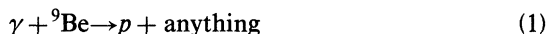
was performed by the use of a tagged photon beam with an energy range between 177 and 417 MeV for the beryllium nucleus, and with an energy range between 337 and 577 MeV for the carbon nucleus. A magnetic spectrometer located at a laboratory angle of 25° was used to detect protons with momenta greater than 300 MeV/c. A schematic view of the experimental setup is shown in Fig. 1.

A. Photon beam and target

The incident photon beam was supplied from a photon tagging system with an energy span of 240 MeV which was divided into 10 MeV bins by 24 tagging counters

$$[(\,\mathrm{TAG})_i,\ i = 1,2,\ldots,24]\ .$$

Details of the system have already been published elsewhere.[1] For the present experiment, four energy bins of the tagging counter were grouped together in each experiment to get the resultant 40 MeV energy bin width. The energy of the tagged photon was calibrated by use of a pair spectrometer with an error less than 5 MeV. The beam size of the tagged photon was about 10 mm in diameter at the target, located at about 3.5 m downstream from the radiator of the photon tagging system. The intensity of the beam during the run was typically 10^5 photons per second. Two subsidiary monitors were used in the photon beam line in order to ascertain the number of photons. These were the counter telescope located behind the target to measure the total yield of electron-positron pairs from the target, and the thick-walled ionization chamber at the end of the photon beam line to measure the total energy of the bremsstrahlung photons.

The beryllium target was a natural beryllium metal with a density of 1.83 g/cm^3. The size of the Be target was $50 \times 50 \times 5$ mm^3, which was large enough to cover the size of tagged photons. The carbon target was natural solid carbon with a density of 1.68 g/cm^3. The size of the C target was $50 \times 50 \times 10$ mm^3. Both targets were placed at an angle of 45° to the beam line.
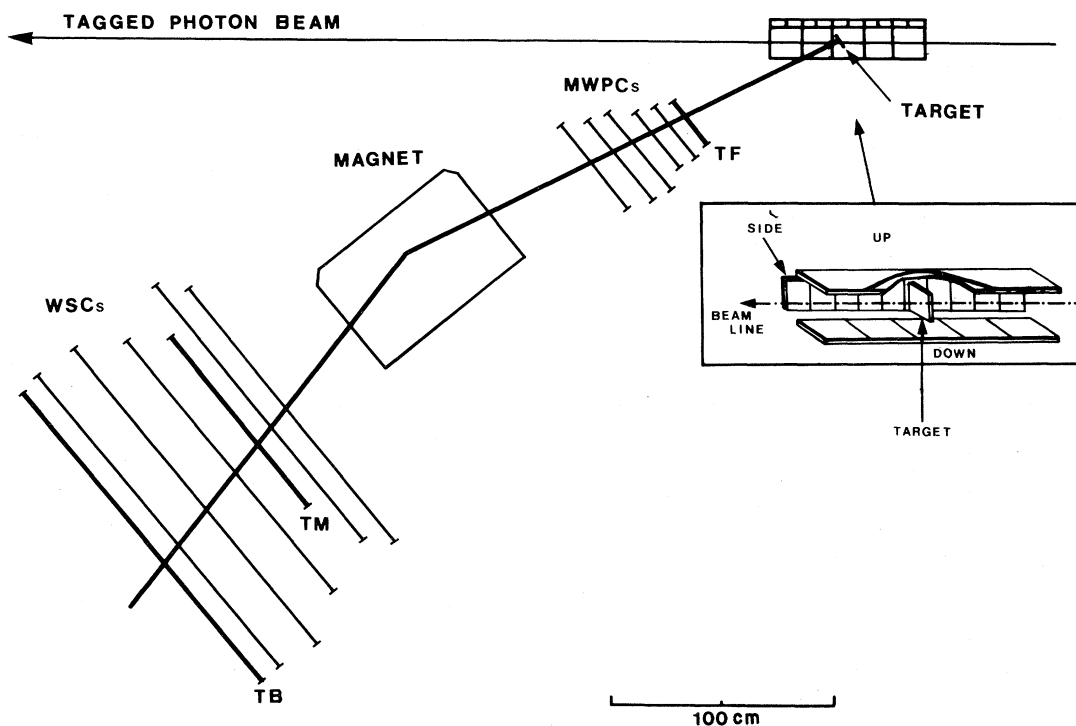

FIG. 1. Experimental apparatus.

B. Spectrometer

The magnetic spectrometer consisted of a bending magnet, three triggering scintillation counters (*TF*, *TM*, and *TB*), five planes of multiwire proportional chambers (MWPC's) (three for horizontal coordinates and two for vertical ones) upstream from the magnet, and five planes of wire spark chambers (WSC's) downstream from the magnet. Each plane of the chamber has an *X-Y* readout system. The momentum calibration of the spectrometer was made within an error of less than 1% by use of an extracted electron beam with a momentum of 700 MeV/*c*, and by use of protons and positive pions from single pion photoproduction from hydrogen in the momentum range between 250 and 1100 MeV/*c*. The angular acceptance of the spectrometer was about ±5° horizontally and ±5° vertically. The momentum resolution, which was a monotonous decreasing function of momentum, was ±2.5% at 500 MeV/*c*, and ±2.0% at 700 MeV/*c*.

The separation of protons from positrons, pions, and deuterons was made by a measurement of the time of flight (TOF) between two triggering counters, *TF* and *TB*, in the spectrometer. Figure 2 shows a typical example of a mass spectrum which was calculated from TOF and momentum measurements, where we see a good separation of protons from other particles.
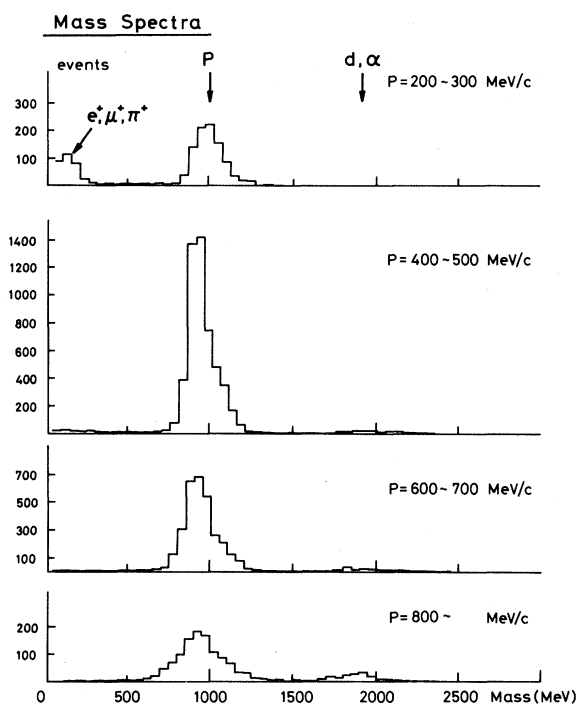

FIG. 2. Mass spectrum of the particles through the spectrometer.

C. Counter telescopes

The target was surrounded by three sets of scintillation counter hodoscopes located 10 cm from the beam line in order to detect charged particles in coincidence with the protons in the spectrometer. The side hodoscope (120×700 mm^2) consisted of ten scintillation counters, and each of the up and down hodoscopes (120×700 mm^2) consisted of five scintillation counters. The back counter which consisted of two scintillation counters was used in coincidence with each hodoscope to reduce background. The hodoscope covered the angular range from 19° to 161° in the production plane and ±80° in the vertical plane. The geometry of the setting of these hodoscopes is seen in Fig. 1.

D. Electronics

A T^*TAG, a coincidence between $T(TF^*TM^*TB)$ and

$$\text{TAG} = \sum_i (\text{TAG})_i \, ,$$

was used as a master triggering signal for the whole electronics system. The triggering signals were fed to CAMAC modules (1) to digitize the positions of the particle hit wires of the MWPC's and WSC's, (2) to start the time to digital converters (TDC's) for the TOF measurements between *TF* and *TB*, and between TAG and *TF*, (3) to open the gate of the analog to digital converter (ADC) for the pulse height measurement of *TF*, and (4) to strobe the input registers for bit information of the scintillation counters.

Data from the CAMAC modules were read into an on-line terminal computer, PANA-FACOM U-400, event by event. This computer stored the raw data on disks and transferred them into a central computer, FACOM M-180II AD, for on-line analyses of the data. Analyzed results were returned to the terminal computer for printing out after the end of each run. Both the raw and analyzed data were stored in magnetic tapes at the central computer for later analyses.

III. DATA REDUCTION

In each of the accumulated events, the particle trajectory was reconstructed using the coordinates measured by the chambers located upstream and downstream from the magnet in order to determine the emission angle and the momentum of the protons. After this, the accepted events were grouped into a momentum bin width of 20 MeV/*c*. This bin width was chosen to be comparable to the momentum resolution of the spectrometer. The accepted events were also grouped into an incident energy bin

of 40 MeV.

Various corrections were made on the raw data in the process of calculating the differential cross sections. The efficiency of the trajectory reconstruction was about 93% at 500 MeV/c and about 90% at 800 MeV/c. Most of the rejected events came from multiple firings and/or no firings in proportional or spark chambers. Accidental coincidence was 15% for T^*TAG. The accidental countings were corrected using the TOF spectrum between T and TAG. The pion and deuteron contamination in the proton events were estimated at less than 1%. The counting rate without the target was less than 0.5% of the rate with the target after the cut in the reaction point was made. The nuclear absorption corrections at the target and spectrometer were about 4% at 400 MeV/c and about 2% at momentum greater than 600 MeV/c.

After the above corrections were made on the raw data, the differential cross sections of reactions (1) and (2) were calculated from the proton yield Y_p by the following equation:

$$\frac{d^2\sigma}{dp_p d\Omega_p} = \frac{Y_p}{N_\gamma N_T \Delta p \Delta\Omega} \ ,$$

where N_γ was the number of incident photons, N_T was the number of target nuclei per cm^2, Δp was the momentum bin width, and $\Delta\Omega$ was the solid angle of the spectrometer. The solid angle of the spectrometer was calculated by a Monte Carlo method, which took account of the detector geometry, energy losses in the materials, the scattering in and out due to the multiple Coulomb effect, and the distribution of the magnetic field.

IV. RESULTS AND DISCUSSION

The momentum spectra of protons from reactions (1) and (2) are shown in Figs. 3 and 4 for various energies of incident photons. The numerical values of the cross sections are listed in Table I. The errors attached to the values of the cross sections are only statistical ones. The systematic errors are listed in Table II.

At energies greater than 300 MeV, the momentum spectra have apparently two broad peaks for reaction (1). Below 300 MeV, one of the peaks extends below the minimum momentum acceptance of the spectrometer. For reaction (2) the structure with these two peaks is not as distinct as the case for reaction (1). Especially above 460 MeV, the lower momentum part of the spectrum rises to smear the low momentum peak and the height of the high momentum peak decreases as the photon energy increases, so that the whole spectrum becomes structureless.
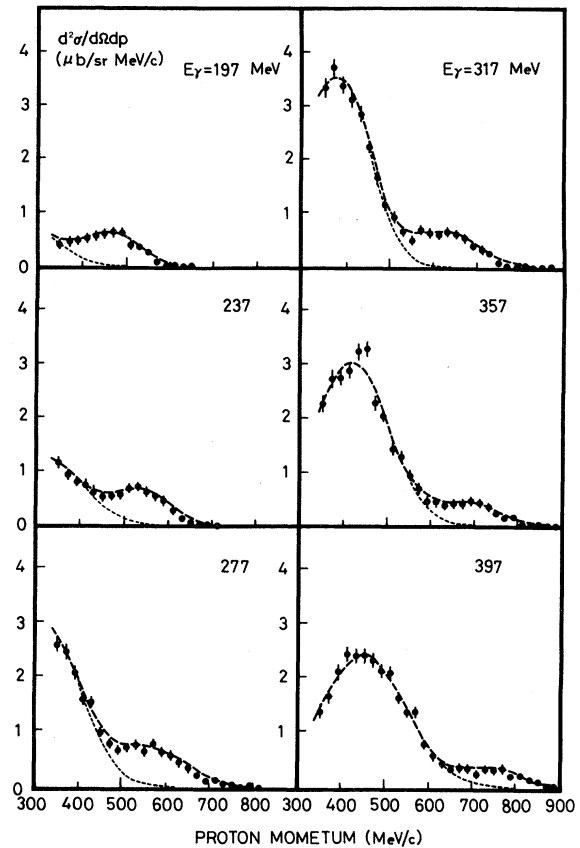

FIG. 3. Momentum spectra of the protons at the laboratory angle $25°\pm5°$ in the reaction $\gamma + \text{Be} \rightarrow p + \text{anything}$. The broken curves are fits of the spectrum, assuming two Gaussian distributions.

The variation of the peak at lower momentum (first peak) as a function of photon energy suggests, as seen in Fig. 5, that the protons in this peak come mainly from the recoil protons in the reactions,

$$\gamma + \text{``}p\text{''} \rightarrow p + \pi^0 \tag{3}$$

and

$$\gamma + \text{``}n\text{''} \rightarrow p + \pi^- \ , \tag{4}$$

where "p" and "n" denote the quasifree protons and neutrons in the nucleus. For the other peak at higher momentum (second peak), its variation as a function of photon energy suggests, as seen in Fig. 5, that the protons in this peak come mainly from the reaction,

$$\gamma + \text{``}pN\text{''} \rightarrow p + N \ , \tag{5}$$

where N denotes the nucleons, and "pN" denotes the quasifree proton-proton or proton-neutron systems in the nucleus. The differences in the observed location of the first and second peaks from the one of
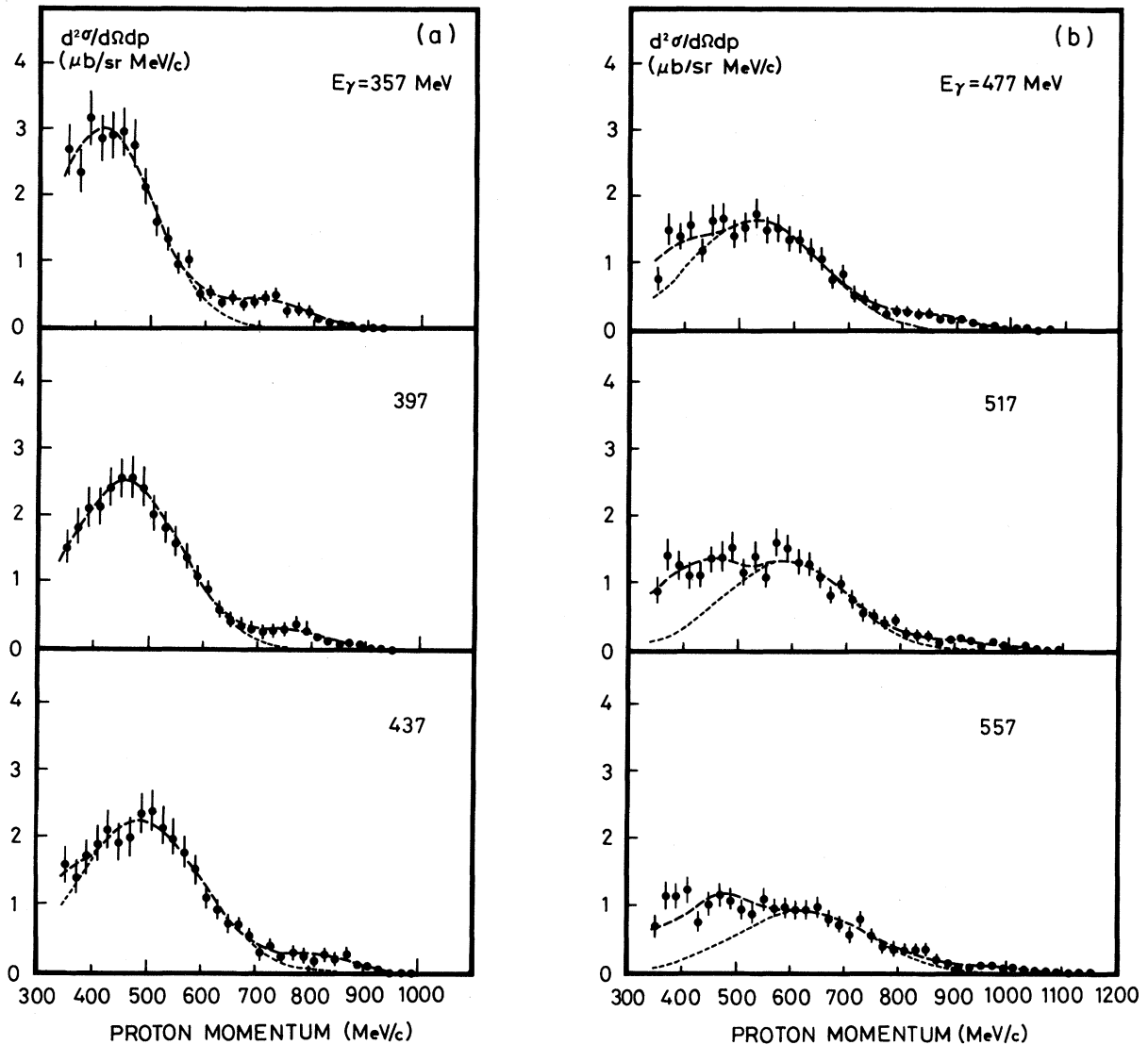
FIG. 4. Momentum spectra of the protons at the laboratory angle $25° \pm 5°$ in the reaction $\gamma + C \rightarrow p +$ anything. The broken curves are fits of the spectrum, assuming two Gaussian distributions and one three-body phase space.

the corresponding free target kinematics (solid and broken lines in Fig. 5) are qualitatively understood to be due to the binding effects of the quasifree targets, nucleons and p-N systems.

The rise in the low momentum part of the spectrum at higher incident energies for carbon suggests that there might be some contribution from the double pion production from the quasifree nucleons in the nucleus,

$$\gamma + \text{``}N\text{''} \rightarrow p + \pi + \pi \ . \tag{6}$$

The analysis of the spectrum was, therefore, performed by use of two Gaussian-type distributions corresponding to the quasifree two-body reactions

(3) plus (4) and (5), and of a three body phase space corresponding to reaction (6). The results of this analysis are shown in Figs. 3 and 4 by broken curves and listed in Table III for beryllium and carbon.

In order to investigate the pN systems in reaction (5), the hodoscope information was used. As shown in Fig. 6, the second peak almost disappears when coincidence between the spectrometer and any one of the hodoscopes is required. The ratio of the hodoscope-fired events to the total was about 3—8 %. This is in good agreement with the carbon data by Arends et al.[6] and is consistent with the prediction by Wakamatsu and Matsumoto.[15] Therefore, the second peak is mainly due to the photo-

S. HOMMA *et al.*

TABLE I. The cross sections.

$\gamma + {}^9\text{Be} \to p + \text{anything}$					
Photon energy (MeV)	Proton momentum (MeV/c)	Cross section $d^2\sigma/d\Omega\,dp$ (μb/sr MeV/c)	Photon energy (MeV)	Proton momentum (MeV/c)	Cross section $d^2\sigma/d\Omega\,dp$ (μb/sr MeV/c)
197	350	0.414±0.063		650	0.342±0.049
	370	0.459±0.062		670	0.224±0.040
	390	0.492±0.061		690	0.110±0.031
	410	0.517±0.060		710	0.105±0.029
	430	0.563±0.060		730	0.056±0.023
	450	0.602±0.059		750	0.045±0.020
	470	0.643±0.058		770	0.017±0.017
	490	0.632±0.056		790	0.028±0.015
	510	0.395±0.046		810	0.006±0.010
	530	0.349±0.044		830	0.000±0.011
	550	0.254±0.040			
	570	0.073±0.027	317	350	3.346±0.175
	590	0.022±0.023		370	3.730±0.175
	610	0.013±0.019		390	3.393±0.161
	630	0.009±0.016		410	3.135±0.151
	650	0.009±0.018		430	2.862±0.141
				450	2.250±0.122
237	350	1.171±0.104		470	1.658±0.102
	370	0.937±0.090		490	1.168±0.085
	390	0.818±0.082		510	0.928±0.077
	410	0.761±0.078		530	0.666±0.067
	430	0.608±0.069		550	0.520±0.062
	450	0.533±0.063		570	0.712±0.069
	470	0.540±0.060		590	0.647±0.066
	490	0.566±0.059		610	0.608±0.065
	510	0.700±0.065		630	0.668±0.067
	530	0.715±0.064		650	0.612±0.064
	550	0.616±0.062		670	0.527±0.059
	570	0.539±0.058		690	0.403±0.052
	590	0.469±0.055		710	0.333±0.047
	610	0.279±0.045		730	0.274±0.043
	630	0.149±0.035		750	0.110±0.027
	650	0.059±0.027		770	0.061±0.023
	670	0.027±0.021		790	0.012±0.012
	690	0.000±0.015		810	0.025±0.015
	710	0.005±0.014		830	0.000±0.009
				850	0.025±0.012
277	350	2.617±0.151		870	0.006±0.006
	370	2.482±0.140			
	390	2.075±0.125	357	350	2.261±0.151
	410	1.612±0.109		370	2.743±0.157
	430	1.564±0.104		390	2.745±0.150
	450	1.009±0.083		410	2.880±0.149
	470	0.790±0.073		430	3.240±0.153
	490	0.675±0.066		450	3.276±0.149
	510	0.705±0.068		470	2.267±0.122
	530	0.781±0.070		490	2.046±0.113
	550	0.656±0.066		510	1.429±0.095
	570	0.791±0.070		530	1.314±0.092
	590	0.650±0.064		550	0.958±0.081
	610	0.577±0.063		570	0.695±0.070
	630	0.449±0.054		590	0.481±0.060

TABLE I. *(Continued.)*

$\gamma + {}^{9}\text{Be} \rightarrow p + \text{anything}$

Photon energy (MeV)	Proton momentum (MeV/c)	Cross section $d^2\sigma/d\Omega\,dp$ (μb/sr MeV/c)	Photon energy (MeV)	Proton momentum (MeV/c)	Cross section $d^2\sigma/d\Omega\,dp$ (μb/sr MeV/c)
	610	0.462±0.060		470	2.343±0.132
	630	0.392±0.055		490	2.148±0.124
	650	0.419±0.056		510	2.118±0.123
	670	0.422±0.055		530	1.663±0.110
	690	0.481±0.058		550	1.401±0.103
	710	0.446±0.055		570	1.398±0.103
	730	0.365±0.051		590	0.814±0.079
	750	0.244±0.040		610	0.563±0.070
	770	0.168±0.035		630	0.434±0.062
	790	0.149±0.032		650	0.322±0.054
	810	0.052±0.021		670	0.367±0.056
	830	0.026±0.016		690	0.347±0.054
	850	0.007±0.011		710	0.262±0.047
	870	0.013±0.009		730	0.337±0.053
	890	0.007±0.007		750	0.331±0.051
				770	0.347±0.051
397	350	1.390±0.132		790	0.222±0.042
	370	1.671±0.135		810	0.244±0.044
	390	2.116±0.144		830	0.134±0.033
	410	2.464±0.150		850	0.082±0.027
	430	2.420±0.143		870	0.015±0.010
	450	2.418±0.139		890	0.015±0.010

$\gamma + {}^{12}\text{C} \rightarrow p + \text{anything}$

Photon energy (MeV)	Proton momentum (MeV/c)	Cross section $d^2\sigma/d\Omega\,dp$ (μb/sr MeV/c)	Photon energy (MeV)	Proton momentum (MeV/c)	Cross section $d^2\sigma/d\Omega\,dp$ (μb/sr MeV/c)
357	350	2.722±0.361		790	0.229±0.052
	370	2.338±0.333		810	0.144±0.049
	390	3.162±0.397		830	0.106±0.034
	410	2.860±0.357		850	0.058±0.024
	430	2.913±0.360		870	0.049±0.022
	450	2.974±0.365		890	0.010±0.010
	470	2.775±0.331		910	0.019±0.014
	490	2.132±0.279		930	0.010±0.010
	510	1.593±0.213			
	530	1.351±0.182	397	350	1.517±0.240
	550	0.963±0.150		370	1.840±0.268
	570	1.025±0.144		390	2.114±0.290
	590	0.533±0.098		410	2.123±0.282
	610	0.564±0.104		430	2.416±0.306
	630	0.408±0.080		450	2.543±0.319
	650	0.472±0.098		470	2.570±0.320
	670	0.368±0.077		490	2.417±0.297
	690	0.408±0.077		510	2.016±0.254
	710	0.477±0.085		530	1.806±0.231
	730	0.498±0.088		550	1.587±0.206
	750	0.275±0.063		570	1.381±0.185
	770	0.294±0.060		590	1.089±0.152

TABLE I. (*Continued.*)

Photon energy (MeV)	Proton momentum (MeV/c)	Cross section $d^2\sigma/d\Omega\,dp$ (μb/sr MeV/c)	Photon energy (MeV)	Proton momentum (MeV/c)	Cross section $d^2\sigma/d\Omega\,dp$ (μb/sr MeV/c)
	610	0.904±0.132	477	350	0.779±0.174
	630	0.609±0.099		370	1.505±0.238
	650	0.438±0.085		390	1.404±0.214
	670	0.380±0.075		410	1.556±0.224
	690	0.308±0.069		430	1.191±0.185
	710	0.263±0.061		450	1.644±0.229
	730	0.265±0.063		470	1.672±0.227
	750	0.308±0.068		490	1.421±0.201
	770	0.379±0.075		510	1.537±0.210
	790	0.289±0.064		530	1.735±0.223
	810	0.156±0.046		550	1.452±0.196
	830	0.125±0.044		570	1.521±0.199
	850	0.094±0.036		590	1.366±0.183
	870	0.126±0.039		610	1.316±0.176
	890	0.084±0.031		630	1.203±0.163
	910	0.032±0.019		650	1.081±0.151
	930	0.042±0.022		670	0.772±0.119
	950	0.000±0.016		690	0.849±0.126
				710	0.561±0.095
437	350	1.611±0.246		730	0.495±0.089
	370	1.424±0.250		750	0.378±0.074
	390	1.728±0.263		770	0.236±0.057
	410	1.911±0.273		790	0.276±0.063
	430	2.130±0.280		810	0.289±0.065
	450	1.938±0.271		830	0.235±0.055
	470	2.001±0.268		850	0.257±0.060
	490	2.352±0.298		870	0.151±0.043
	510	2.400±0.297		890	0.151±0.043
	530	2.170±0.272		910	0.162±0.045
	550	2.010±0.251		930	0.108±0.036
	570	1.807±0.232		950	0.054±0.025
	590	1.536±0.202		970	0.065±0.032
	610	1.116±0.163		990	0.022±0.016
	630	0.942±0.138		1010	0.054±0.025
	650	0.732±0.117		1030	0.043±0.022
	670	0.729±0.113		1050	0.000±0.010
	690	0.530±0.103		1070	0.011±0.011
	710	0.299±0.077			
	730	0.412±0.079	517	350	0.889±0.185
	750	0.254±0.065		370	1.417±0.229
	770	0.316±0.069		390	1.273±0.208
	790	0.253±0.071		410	1.113±0.191
	810	0.192±0.065		430	1.125±0.181
	830	0.266±0.060		450	1.346±0.199
	850	0.213±0.057		470	1.397±0.203
	870	0.269±0.060		490	1.516±0.209
	890	0.108±0.042		510	1.168±0.168
	910	0.097±0.034		530	1.408±0.195
	930	0.065±0.027		550	1.091±0.159
	950	0.000±0.023		570	1.598±0.209
	970	0.011±0.025		590	1.518±0.198
	990	0.011±0.011		610	1.310±0.179

TABLE I. (*Continued.*)

$\gamma + {}^{12}C \rightarrow p +$ anything

Photon energy (MeV)	Proton momentum (MeV/c)	Cross section $d^2\sigma/d\Omega\,dp$ (μb/sr MeV/c)	Photon energy (MeV)	Proton momentum (MeV/c)	Cross section $d^2\sigma/d\Omega\,dp$ (μb/sr MeV/c)
	630	1.293±0.174		510	0.958±0.150
	650	1.092±0.152		530	0.895±0.142
	670	0.837±0.129		550	1.107±0.162
	690	1.003±0.144		570	0.977±0.144
	710	0.763±0.120		590	0.999±0.145
	730	0.566±0.098		610	0.957±0.140
	750	0.519±0.092		630	0.956±0.143
	770	0.423±0.083		650	1.006±0.143
	790	0.460±0.085		670	0.832±0.125
	810	0.226±0.058		690	0.727±0.117
	830	0.249±0.059		710	0.590±0.101
	850	0.238±0.057		730	0.818±0.126
	870	0.114±0.042		750	0.569±0.098
	890	0.172±0.050		770	0.410±0.083
	910	0.195±0.054		790	0.368±0.079
	930	0.172±0.048		810	0.360±0.077
	950	0.069±0.037		830	0.360±0.075
	970	0.137±0.042		850	0.383±0.076
	990	0.069±0.029		870	0.216±0.057
	1010	0.023±0.016		890	0.148±0.047
	1030	0.092±0.034		910	0.102±0.039
	1050	0.034±0.020		930	0.091±0.037
	1070	0.011±0.012		950	0.125±0.040
	1090	0.011±0.012		970	0.125±0.040
				990	0.080±0.031
557	350	0.712±0.166		1010	0.102±0.036
	370	1.158±0.209		1030	0.080±0.031
	390	1.160±0.193		1050	0.034±0.020
	410	1.235±0.192		1070	0.046±0.023
	430	0.776±0.153		1090	0.023±0.016
	450	1.032±0.170		1110	0.011±0.011
	470	1.177±0.181		1130	0.000±0.010
	490	1.105±0.167		1150	0.011±0.011

TABLE II. Systematic errors.

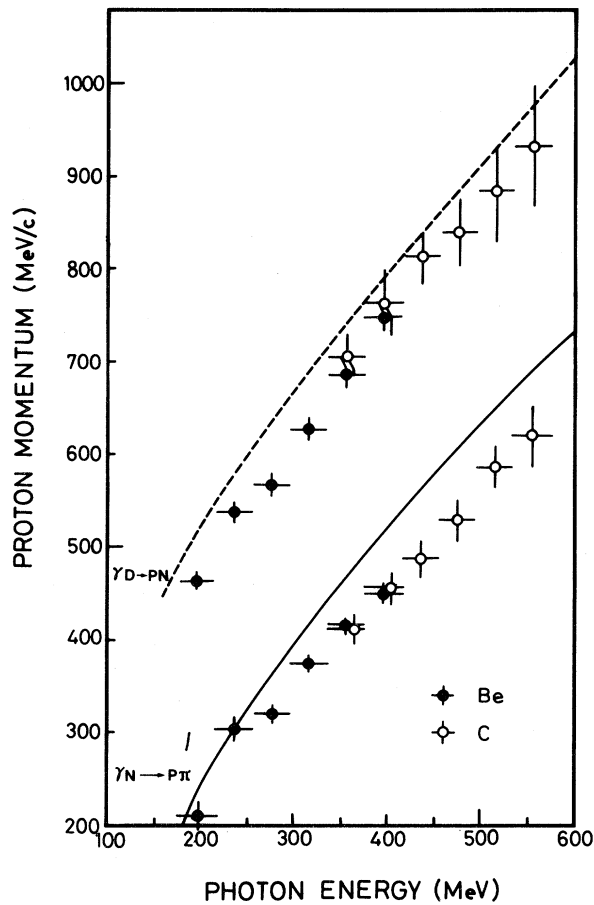|	
Number of tagged photons	±4.6%
Number of target nuclei	±2.0%
Acceptance of spectrometer	±4.3%
Momentum calibration	±0.8%
Empty target subtraction	±1.0%
Accidental coincidence	< ±0.8%
Nuclear absorption	< ±5.0%
Storage efficiency	±0.8%
Trajectory reconstruction efficiency	±3.5%
Proton identification	$\left\{ \begin{array}{l} +1.0\% \\ -2.8\% \end{array} \right.$
Quadratic sum	$\left\{ \begin{array}{l} +9.2\% \\ -9.8\% \end{array} \right.$

FIG. 5. Photon energy dependence of the location of two peaks in the momentum spectrum. The solid line indicates kinematics of the pion photoproduction from a free nucleon, and the broken line, the photodisintegration of free deuterons.
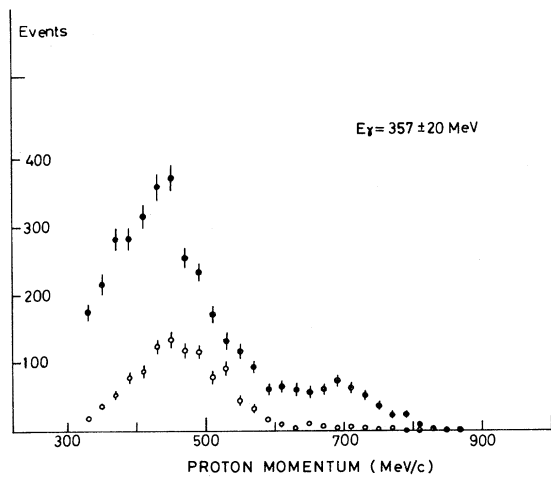

FIG. 6. Momentum spectrum of the protons at $E_\gamma = 357 \pm 20$ MeV. The solid circles represent the reaction $\gamma + Be \rightarrow p +$ anything, and open circles, the reaction $\gamma + Be \rightarrow p + ($ charged particle $) +$ anything.
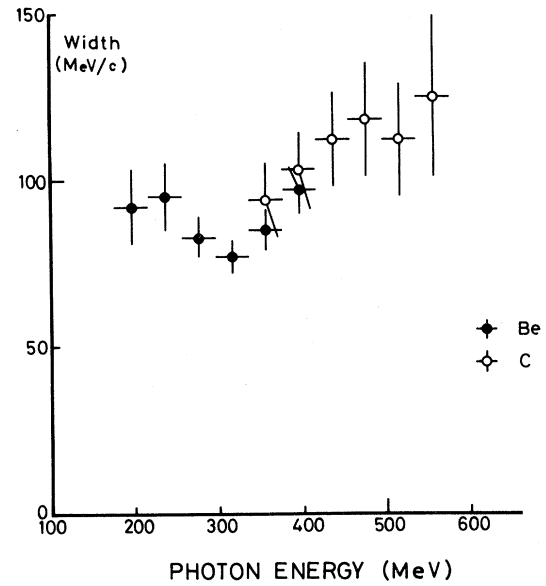
FIG. 7. The width of the first peak in the momentum spectrum of protons from ^9Be and ^{12}C, closed circles for ^9Be and open circles for ^{12}C.

disintegration of the proton-neutron systems in the nucleus,

$$\gamma + \text{"}pn\text{"} \rightarrow p + n \ . \tag{5a}$$

The first peak in the low momentum part of the spectrum was decreased in height, but still existed when the above coincidence was required. This is
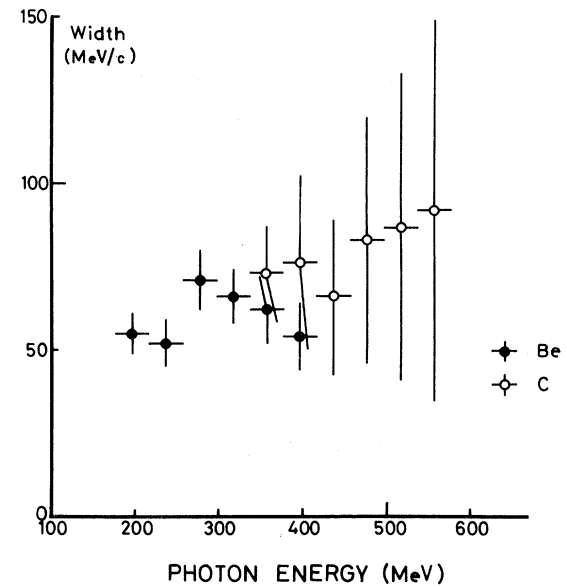

FIG. 8. The width of the second peak in the momentum spectrum of protons from ^9Be and ^{12}C, closed circles for ^9Be and open circles for ^{12}C.

TABLE III. Values obtained by two Gaussian fitting of momentum spectrum. Upper half: two Gaussian fittings: $d^2\sigma/d\Omega\,dp = \sum_{i=1}^{2} a_i \exp\{-(p-p_0^i)^2/2\sigma_i^2\}$. Lower half: two Gaussian plus three body phase space: $d^2\sigma/d\Omega\,dp = \sum_{i=1}^{2} a_i \exp\{-(p-p_0^i)^2/2\sigma_i^2\} + a_3 \times$ three-body phase space, where $\int_0^{p^{max}}$ (three-body phase space) $dp = 1$.

				$\gamma + {}^9\text{Be} \rightarrow p + \text{anything}$				
E_γ (MeV)	$\chi^2/d.f.$	a_1 (μb/sr MeV/c)	p_0^1 (MeV/c)	σ_1 (MeV/c)	a_2 (μb/sr MeV/c)	p_0^2 (MeV/c)	σ_2 (MeV/c)	
197 ± 20	1.11	1.23 ± 0.40	213 ± 17	92 ± 11	0.621 ± 0.079	465 ± 8	55 ± 6	
237 ± 20	0.35	1.26 ± 0.19	305 ± 13	95 ± 10	0.637 ± 0.098	540 ± 10	52 ± 7	
277 ± 20	0.93	2.94 ± 0.31	320 ± 9	83 ± 6	0.681 ± 0.104	568 ± 12	71 ± 9	
317 ± 20	0.98	3.57 ± 0.30	375 ± 7	77 ± 5	0.660 ± 0.115	628 ± 12	66 ± 8	
357 ± 20	1.37	3.05 ± 0.24	415 ± 8	85 ± 6	0.444 ± 0.100	687 ± 15	62 ± 10	
397 ± 20	1.07	2.46 ± 0.20	449 ± 10	97 ± 7	0.330 ± 0.100	751 ± 16	54 ± 10	

|				$\gamma + {}^{12}\text{C} \rightarrow p + \text{anything}$				
E_γ (MeV)	$\chi^2/d.f.$	a_1 (μb/sr MeV/c)	p_0^1 (MeV/c)	σ_1 (MeV/c)	a_2 (μb/sr MeV/c)	p_0^2 (MeV/c)	σ_2 (MeV/c)	a_3 (μb/sr MeV/c)
357 ± 20	0.60	3.02 ± 0.53	412 ± 16	94 ± 11	0.410 ± 0.131	708 ± 23	73 ± 14	
397 ± 20	0.48	2.50 ± 0.40	454 ± 16	103 ± 11	0.237 ± 0.102	764 ± 34	76 ± 26	
437 ± 20	0.59	2.26 ± 0.40	487 ± 20	112 ± 14	0.235 ± 0.116	820 ± 30	66 ± 23	2.68 ± 6.81
477 ± 20	0.76	1.63 ± 0.32	529 ± 24	118 ± 17	0.170 ± 0.097	839 ± 37	83 ± 37	3.03 ± 3.43
517 ± 20	0.97	1.35 ± 0.28	586 ± 25	112 ± 17	0.133 ± 0.086	885 ± 54	87 ± 46	5.72 ± 2.89
557 ± 20	1.09	0.92 ± 0.22	621 ± 35	125 ± 24	0.093 ± 0.072	933 ± 66	92 ± 57	5.16 ± 2.54
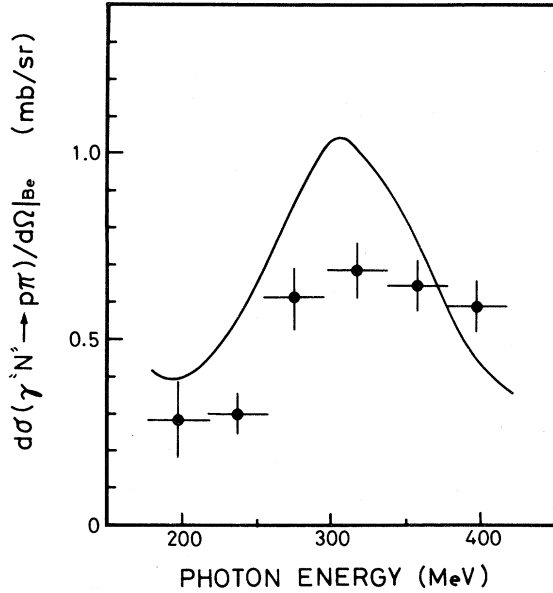
FIG. 9. The integrated cross sections

$d\sigma(\gamma + \text{"}N\text{"} \rightarrow p + \pi)/d\Omega\,|_{\text{Be}}$

as a function of photon energy. The solid line is a sum of the cross sections of the photoproduction of pions from a free nucleon target,

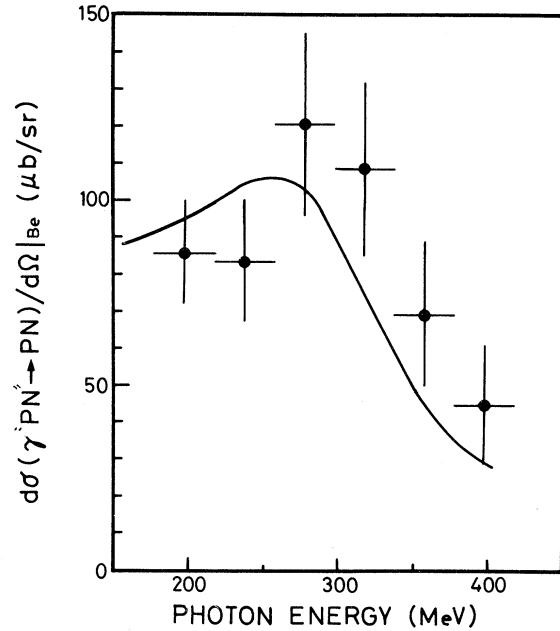$Z \cdot d\sigma(\gamma + p \rightarrow p + \pi^0)/d\Omega + N\,d\sigma(\gamma + n \rightarrow p + \pi^-)/d\Omega$.

FIG. 10. The integrated cross sections

$d\sigma(\gamma + \text{"}pn\text{"} \rightarrow p + n)/d\Omega\,|_{\text{Be}}$

as a function of photon energy. The solid curve is

$11 \times d\sigma(\gamma + d \rightarrow p + n)/d\Omega\,|_{\text{free}}$

for similar kinematical conditions.

qualitatively explained by the idea that reaction (4) is separated from reaction (3) by requiring the emission of the charged particles at the opposite side of the protons.

The widths of the first and second peaks are shown in Figs. 7 and 8 as a function of photon energy. The width of the second peak is narrower than the first. The width of the carbon target is nearly equal to the width of the beryllium target both for the first and second peaks. These widths reflect the internal motion of the quasifree particles in the nucleus. Homma and Tezuka[16] analyzed the second peak of reaction (5a) and obtained a good fit to the observed width when they assumed 200 MeV/c as a width of the Gaussian-type momentum distribution of the p-n systems inside the nucleus. Their value is very close to phenomenological estimates.[17]

The cross sections $d\sigma/d\Omega$ for the reactions (3) plus (4) and (5a) are obtained by integrating the corresponding Gaussian distribution over the proton momentum. The results are shown in Figs. 9 and 10 for beryllium and Figs. 11 and 12 for carbon as a function of incident photon energy. The integrated
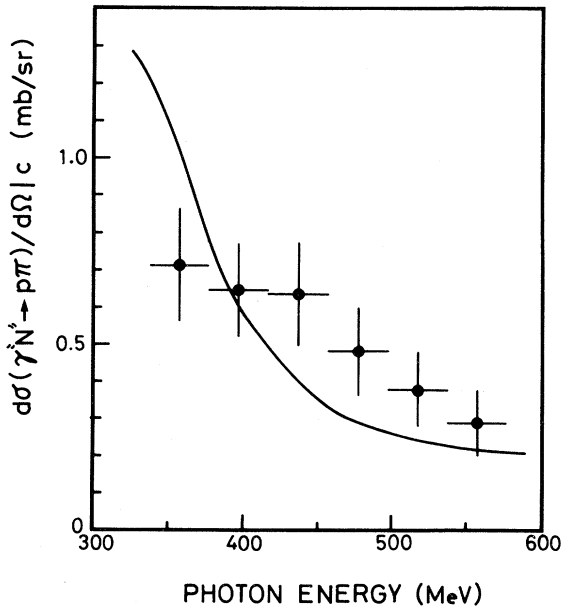

FIG. 12. The integrated cross sections

$$d\sigma(\gamma + ``pn" \rightarrow p + n)d\Omega \mid_C$$

as a function of photon energy. The solid curve is

$$14 \times d\sigma(\gamma + d \rightarrow p + n)/d\Omega \mid_{free}$$

for similar kinematical conditions.

FIG. 11. The integrated cross sections

$$d\sigma(\gamma + ``N" \rightarrow p + \pi)/d\Omega \mid_C$$

as a function of photon energy. The solid line is a sum of the cross sections of the photoproduction of pions from a free nucleon target,

$$Z \cdot d\sigma(\gamma + p \rightarrow p + \pi^0)/d\Omega + N \, d\sigma(\gamma + n \rightarrow p + \pi^-)/d\Omega \; .$$
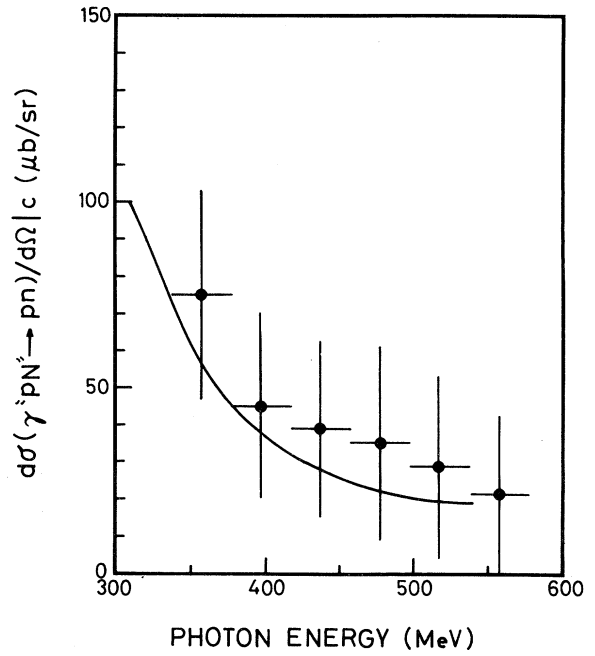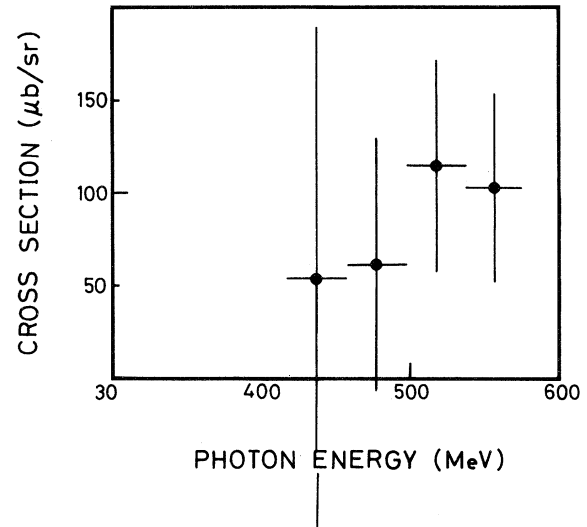

FIG. 13. The integrated cross sections

$$\int \{d^2\sigma(\gamma + ``N" \rightarrow p + \pi + \pi)/dp\,d\Omega\}_C dp$$

for carbon as a function of photon energy.

TABLE IV. Integrated cross sections.

$\gamma + {}^9\mathrm{Be} \rightarrow p + $ anything

Photon energy (MeV)	Cross section (first peak) $d\sigma/d\Omega$ (μb/sr)	Cross section (second peak) $d\sigma/d\Omega$ (μb/sr)
197±20	283.9±98.4	85.7±14.1
237±20	299.5±55.7	83.6±16.6
277±20	613.0±80.2	120.4±24.4
317±20	686.5±73.8	108.4±23.2
357±20	647.4±68.9	69.0±19.4
397±20	596.4±66.8	44.9±16.0

$\gamma + {}^{12}\mathrm{C} \rightarrow p + $ anything

Photon energy (MeV)	Cross section (first peak) $d\sigma/d\Omega$ (μb/sr)	Cross section (second peak) $d\sigma/d\Omega$ (μb/sr)	Cross section (three-body space) $d\sigma/d\Omega$ (μb/sr)
357±20	711.6±150.5	75.0±28.1	
397±20	645.5±122.6	45.1±24.9	
437±20	634.5±136.0	38.9±23.5	53.6±136.1
477±20	482.1±118.1	35.4±25.8	60.6±68.5
517±20	379.0±99.0	29.0±24.2	114.4±57.9
557±20	288.3±88.4	21.4±21.2	103.2±50.7

cross sections for the three-body reaction (6) is also plotted in Fig. 13 as a function of incident energy. The numerical values of the integrated cross sections are listed in Table IV.

In the quasifree two body reactions (3) plus (4), and (5a), the cross sections show the broad peak structure around 300 MeV, which is due to the Δ excitation in both of the reactions for the beryllium target. The energy region for carbon in the present experiment is beyond the Δ region, so that a monotonously decreasing tendency with increasing energy is observed for both reactions (3) plus (4) and (5a). The integrated cross sections for reaction (6) rise from around 400 MeV, which corresponds to the threshold of the double pion production. The double pion production is almost the main contributor at the low energy part of the spectrum above 400 MeV for the carbon target.

The photon energy dependence of the cross section for reactions (3) plus (4) shows a broad peak at about 300 MeV for the beryllium target, and a monotonous decreasing tendency as the energy increases for the carbon target, as seen in Figs. 9 and 11. The solid curves in the figures are the sum of the cross sections for the elementary processes,

$$\gamma + p \rightarrow p + \pi^0 \tag{7}$$

and

$$\gamma + n \rightarrow p + \pi^- \tag{8}$$

in the following way:

$$Z \cdot \left. \frac{d\sigma}{d\Omega} \right|_{(7)} + N \cdot \left. \frac{d\sigma}{d\Omega} \right|_{(8)}. \tag{9}$$

Since the mass of the nucleons in the nucleus is lighter than the mass of the free nucleons, the center of mass energy for the nucleon target in the nucleus is lower than that of the free nucleons even when the incident photon energy is the same. Therefore, we have to correct for this effect when we compare the present experimental cross sections with the ones of the free nucleon target. This is simply done by shifting the curves by about 30 MeV to the higher energy side. If we do this, the experimental cross sections are qualitatively reproduced by these curves for both the beryllium and the carbon targets, although the cross sections are slightly lower than the curve at the Δ region for the beryllium target.

As shown in Figs. 3 and 4, the existence of the second peak in the high momentum part of the spectrum is as clear as the first peak. Therefore, if we can say that there exist almost-independent nucleons (quasifree nucleons) in the nucleus from the existence of the first peak in the momentum spectrum, for the same reason we can say there exist almost-independent p-n pairs (quasifree p-n pairs) in the nu-

cleus from the existence of the second peak in the spectrum, or at least we can say that there is a strong *p-n* correlation in the nucleus. Although Mecking[6] and Arends *et al.*[7] observed clear evidence of the existence of *p-n* correlation by measuring the relative emission angle between protons and neutrons from carbon, and observed an enhancement of the event at the region of our second peak in the momentum spectrum of protons, they could not obtain a clear peak such as ours, indicating the apparent existence of the quasifree *p-n* pairs. This may be because they measured the proton spectrum at larger angles where one might expect more smearing due to final state interactions.

In the analysis of the present cross sections for reaction (5a), the simplest way is to compare them with the cross sections of free deuterons. The cross sections for free deuterons in a similar kinematical condition to ours ($\theta_p^* = 31°-35°$) were measured by Dougan *et al.*[8] ($\theta_p^* = 37°$). The solid lines in Figs. 10 and 12 represent the measured free deuteron differential cross sections multiplied by a factor of 11 for beryllium and 14 for carbon. These factors were determined to obtain a good eye fit to our cross sections. The photon energy dependence of the cross sections for reaction (5a) in both targets is very close to the one for free deuterons when the energy scale is shifted by an amount of about 30 MeV to higher values. This energy shift is understood in the difference of the center of mass energy due to the binding of the quasifree *p-n* system to the nucleus, even when the photon energy is the same. The similarity of the photon energy dependence in the cross section of the photodisintegration of quasifree *p-n* pairs with the dependence of free deuterons suggests that the wave function describing the quasifree *p-n* pairs may be very close to the wave function of deuterons in the short distances, which contributes to the cross section in our energy region.

According to Levinger's quasideuteron model,[3] the total absorption cross section σ_T of photons in the nucleus is related to the total cross section σ_T^D of photodisintegration of deuterons in the following:

$$\sigma_T = L\frac{ZN}{A}\sigma_T^D , \qquad (10)$$

where ZN is the possible number of *p-n* combinations in a nucleus of mass number A, and L is the Levinger's constant. The ratio LZN/A can be thought of as the effective number of deuteronlike structures which take place in photodisintegration. In the present analysis, we simply parametrize this relation in the following way:

$$\frac{d\sigma}{d\Omega}\bigg|_{"pn"} = L\frac{ZN}{A}\frac{d\sigma}{d\Omega}\bigg|_d . \qquad (11)$$

Using this equation, we obtain $L=5$ for beryllium and for carbon from the present experiment. Although the L value in Eq. (11) has no reason to be equal to the L value of Eq. (10), we can compare the values determined by use of Eq. (11) with the predictions by the quasideuteron model. In the original version of Levinger's model, he deduced $L=6.4$ by using a nuclear radius of $1.4A^{1/3}\times10^{-13}$ cm. Later, he found[9] $L=8$ for a nucleus of radius parameters $r_0=1.2\times10^{-13}$ cm. Recently, Tavares *et al.*[10] analyzed (γ,n) and (γ,p) reactions at intermediate energies and found an empirical formula

$$L=2.1\ln(1.3A) , \qquad (12)$$

where A is a mass number. The L value determined by this formula is consistent with the results of the Mainz[11] and Saclay[12] experiments on total photoabsorption cross sections of various nuclei in the energy range from 40 to 150 MeV. This formula leads to $L=5.2$ for beryllium and 5.8 for carbon, which are very close to our result.

Laget[13] analyzed the present data by the pion's production and reabsorption mechanism in the framework of a modified quasideuteron model and reproduced qualitatively two peaks in the momentum spectrum of the beryllium target at one photon energy. Similar analyses were also performed by Wakamatsu and Matsumoto,[14] and Suzumura and Futami.[15] Contrary to these analyses, Homma and Tezuka[16] analyzed the second peak in the momentum spectrum of the present experiment by the photodisintegration of the quasifree hard *p-n* pairs in the nucleus.

Measurements on the angular distribution, proton-neutron or proton-proton correlations, and A dependence would yield further information on the general feature of the mechanism of the photoemission of protons from the nucleus in the energy region above meson threshold.

ACKNOWLEDGMENTS

*Present address: Department of Physics, University of Tokyo, Tokyo 113, Japan.

[1]S. Arai, S. Homma, A. Itano, T. Inagaki, M. Kasuya, K. Maruyama, T. Miyachi, H. Okuno, A. Sasaki, I. Sato, K. Ukai, and T. Yamakawa, Jpn. J. Appl. Phys. 14, 95 (1975).

[2]J. Arends, J. Eyink, H. Hartmann, A. Hegerath, B. Mecking, G. Nöldeke, and H. Rost, University of Bonn Report BONN-HE-78-19, 1979 (unpublished).

[3]J. S. Levinger, Phys. Rev. 84, 43 (1951).

[4]K. Gottfried, Nucl. Phys. 5, 557 (1958).

[5]S. Homma, M. Kanazawa, K. Maruyama, Y. Murata, H. Okuno, A. Sasaki, and T. Taniguchi, Phys. Rev. Lett. 45, 706 (1980).

[6]B. A. Mecking, in Proceedings of the International Conference on Nuclear Physics with Electromagnetic Interactions, Mainz, 1979, edited by H. Arenhövel and D. Drechsel (Springer, Berlin, 1979), p. 382.

[7]J. Arends, J. Eyink, H. Hartmann, A. Hegerath, B. Mecking, G. Nöldeke, and H. Rost, University of Bonn Report BONN-HE-80-7, 1980 (unpublished).

[8]P. Dougan, T. Kivikas, K. Lugnër, V. Ramsey, and W. Stiefler, Z. Phys. A 276, 55 (1976).

[9]J. S. Levinger, Nuclear Photodisintegration (Oxford University Press, London, 1960).

[10]O. A. P. Tavares, J. D. Pinheiro Filho, V. di Napoli, J. B. Martins, and M. L. Terranova, Centro Brasileiro de Pesquisas Fisicas Report CBPF-A0039/79, 1979 (unpublished).

[11]J. Ahrens, H. Borchert, K. H. Kzock, H. B. Eppler, H. Gimm, H. Gundrum, M. Kröning, P. Riehn, G. Sita Ram, A. Zieger, and B. Ziegler, Nucl. Phys. A251, 479 (1975).

[12]A. Lepretre, H. Beil, R. Bergere, P. Carlos, J. Fagot, A. Veyssiere, J. Ahrens, P. Axel, and U. Kneissl, Phys. Lett. 79B, 43 (1978).

[13]J. M. Laget, in Proceedings of the Workshop on Nuclear Physics with Real and Virtual Photons, Bologna, Italy, 1980, edited by H. Arenhövel and A. M. Saruis (Springer, Berlin, 1981), p. 148.

[14]M. Wakamatsu and K. Matsumoto, Nucl. Phys. (to be published).

[15]J. Suzumura and Y. Futami, Prog. Theor. Phys. (to be published).

[16]S. Homma and H. Tezuka, Institute for Nuclear Study Report-449, 1982 (unpublished).

[17]D. W. Devins, B. L. Scott, and H. H. Forster, Rev. Mod. Phys. 37, 396 (1965); F. H. Heimlich, E. Rössls, M. Köbberling, J. Moritz, K. H. Schmidt, D. Wegener, D. Zeller, J. K. Bienlein, J. Bleckwenn, and H. Dinter, Nucl. Phys. A228, 478 (1974).